

## SUPPORTING INFORMATION

### Ultra-High-Efficiency Near-Infrared Ga<sub>2</sub>O<sub>3</sub>:Cr<sup>3+</sup> Phosphor and Controlling of Phytochrome

Mu-Huai Fang,<sup>a</sup> Gabriel Nicolo A. De Guzman,<sup>b</sup> Zhen Bao,<sup>a</sup> Natalia Majewska,<sup>c</sup>  
Sebastian Mahlik,<sup>c,d</sup> Marek Grinberg,<sup>c</sup> Grzegorz Leniec,<sup>e</sup> Sławomir M. Kaczmarek,<sup>e</sup>  
Chia-Wei Yang,<sup>f</sup> Kuang-Mao Lu,<sup>f</sup> Hwo-Shuenn Sheu,<sup>g</sup> Shu-Fen Hu,<sup>b,\*</sup> and Ru-Shi Liu<sup>a,\*</sup>

<sup>a</sup>*Department of Chemistry, National Taiwan University, Taipei 106, Taiwan*

<sup>b</sup>*Department of Physics, National Taiwan Normal University, Taipei 116, Taiwan*

<sup>c</sup>*Institute of Experimental Physics, Faculty of Mathematic, Physics and Informatics, Gdańsk University, Wita Stwosza  
57, 80-308 Gdańsk, Poland*

<sup>d</sup>*Graduate School of Human and Environmental Studies, Kyoto University, Kyoto 606-8501, Japan*

<sup>e</sup>*Faculty of Mechanical Engineering and Mechatronics, West Pomeranian University of Technology, Szczecin, al.  
Piastow 19, 70-311 Szczecin, Poland*

<sup>f</sup>*Everlight Electronics Co., Ltd., New Taipei City 238, Taiwan*

<sup>g</sup>*National Synchrotron Radiation Research Center, Hsinchu 300, Taiwan*

## EXPERIMENTAL METHODS

**Synthesis of  $\text{Ga}_{2-x}\text{O}_3:x\text{Cr}^{3+}$ .** Gallium oxide ( $\text{Ga}_2\text{O}_3$ , Gredmann, 99.99%), chromium oxide ( $\text{Cr}_2\text{O}_3$ , Merck, 99.9%) were acquired from chemical distributors and were directly utilized for a solid-state reaction method. The starting precursors were stoichiometrically weighed, mixed and carefully grounded in an agate mortar for 30 minutes. The finely grounded precursors were transferred into an alumina crucible and moved into a muffle furnace for the sintering process. The samples were sintered to 1200 °C at a rate of 5 °C for 5 hours and afterward cooled to room temperature. The detailed characterization is listed in the Supporting Information.

**Plant growth experiment.** The 450 nm blue LED was used with the  $\text{Ga}_2\text{O}_3:\text{Cr}^{3+}$  IR phosphors with a driving current of 300 mA. The output of the IR region was 17.5 mW. 18 pieces of LEDs are used and the illuminated area was 631.67 mm x 446.41 mm. The plants were divided into two groups and each group had *Aglaonema* and *P. amboinicus*. Both of the groups were illuminated by the sunlight for 12 hours from 08:00 a.m. to 08:00 p.m. The experimental group was further illuminated by our phosphor-converted IR LED for 12 hours from 08:00 p.m. to 08:00 a.m. The control group wasn't illuminated by the IR LED at the night. The height of the plant was calculated from the stem over the soil to the highest leaf.

**Characterization.** The phase and purity of the as-prepared powder samples were examined by X-ray diffraction (XRD) analysis using a D2 PHASER diffractometer (Bruker) with  $\text{CuK}\alpha$  radiation source ( $\lambda = 1.5418 \text{ \AA}$ ). Synchrotron powder X-ray diffraction pattern of  $\text{Ga}_2\text{O}_3:\text{Cr}^{3+}$  was acquired from the National Synchrotron Radiation Research Center (NSRRC, Taiwan) BL01C2 beamline with the wavelength of 0.82657 Å at room temperature using Debye - Scherrer camera. The pattern then proceeded for Rietveld analysis using Total Pattern Analysis Solutions software (TOPAS 4.2). Room temperature (RT) photoluminescence excitation (PLE) spectra were measured with a FluoroMax-4P spectrofluorometer (Horiba) equipped with a 150 W xenon lamp as an excitation light source and an R928 Hamamatsu photomultiplier as a detector which records PL and PLE spectra in the spectral range of 250 – 850 nm. The temperature dependence photoluminescence spectra (PDPL) and pressure dependence of photoluminescence spectra (PDPL) were measured using an Andor SR-750-D1 spectrometer equipped with a CCD camera (DU420A-OE) with the following laser sources: He-Cd laser with 325 and 442 nm, second harmonic Nd:YAG laser with 532 nm and He-Ne laser with 629 nm. The decay profiles were measured via apparatus for time-resolved spectroscopy which consists of a PG 401/SH optical parametric generator pumped by a PL2251A pulsed YAG:Nd laser (EKSPLA), while the detection part consisted of a 2501S grating spectrometer (Bruker Optics) combined with a C4334-01 streak camera (Hamamatsu). Data were recorded in the form of the streak

images on a 640 by 480 pixel CCD array. Results were transformed into a 2D matrix of streak image using software based on the photon counting algorithm. Decay profiles of luminescence were acquired by integrating the streak image over specified spectral windows. Emission spectra were evaluated by integrating the streak image over time. The high-pressure luminescence measurements were performed in a screw-driven Merrill-Bassett type diamond anvil cell (DAC) with a culets diameter of 0.5 mm. The  $\text{KMgF}_3:0.5\%\text{Eu}^{2+}$  was used as a pressure sensor and polydimethylsiloxane oil was used as a pressure transmitting medium between the gaskets. High-pressure luminescence excitation spectra were acquired using a self-made spectrofluorometer. The excitation part of the device consists of a 150W xenon lamp, an SPM2 monochromator (Carl Zeiss Jena) and an R928P photomultiplier for lamp reference measurement. Besides, the detection part consists of an SPM2 monochromator and an R928P photomultiplier as a signal detector. Scanning electron microscopy was conducted on the SIGMA 300 Essential scanning electron microscope (ZEISS, Graduate Institute of Manufacturing Technology, National Taipei University of Technology) along with the attached energy dispersive X-ray spectrometer (Bruker). IR – LED was fabricated by mixing UV gel (Norland optical adhesive 61, LOT 392; Norland product, Inc. Cranbury, NJ 08512) with  $\text{Ga}_{0.994}\text{O}_3:0.006\text{Cr}^{3+}$  phosphor and smearing the mixed gel onto the 450 nm blue chip. Subsequently, the gel was solidified by irradiating 365 nm UV light. The internal quantum efficiency measurement was done using UV to NIR absolute PL quantum yield spectrometer (C1534 – 12; Hamamatsu photonics K.K.) equipped with NIR PL measurement unit (C13684 – 01; Hamamatsu photonics K.K.) using High power Xe lamp unit (L13685 – 01; Hamamatsu photonics K.K.) together with 475 nm filter for excitation (A13686 – 475). The first derivative of the absorption EPR spectrum was recorded as a function of the applied magnetic field in the range  $B = 10 - 1400$  mT on a conventional X-band Bruker ELEXSYS E 500 CW-spectrometer operating at 9.5 GHz with 100 kHz magnetic field modulation. The temperature dependence of the EPR spectrum was analyzed using nitrogen-flow cryostat Oxford Instruments ESP at the nitrogen temperature range. EPR/NMR program was used to find spin-Hamiltonian parameters and local symmetry of chromium ions. Optimization and normalization of the parameters were performed using the root-mean-squared deviation method.

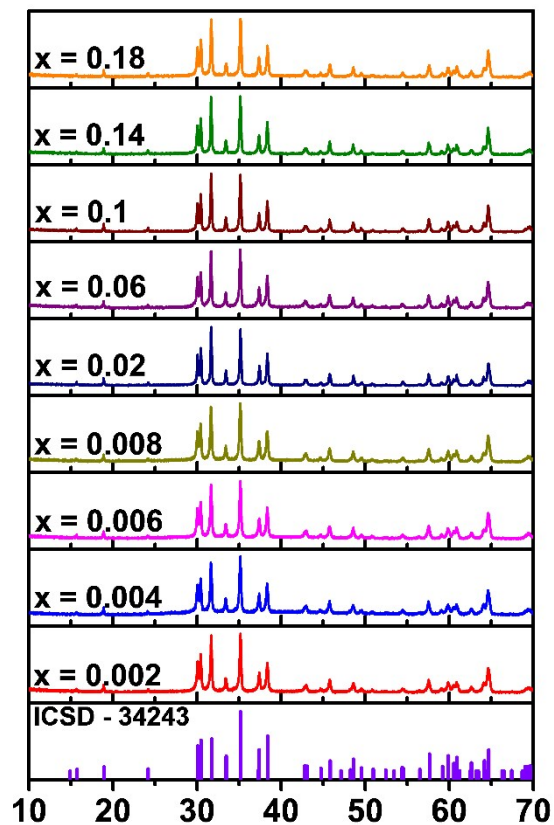


Figure S1. XRD of the  $\text{Ga}_{2-x}\text{O}_3:\text{xCr}^{3+}$  ( $x = 0 - 0.18$ ).

Table S1. IQE of the  $\text{Ga}_{2-x}\text{O}_3:\text{xCr}^{3+}$  ( $x = 0 - 0.18$ ).

<b>x =</b>	<b>0.002</b>	<b>0.004</b>	<b>0.006</b>	<b>0.008</b>	<b>0.02</b>	<b>0.06</b>	<b>0.1</b>	<b>0.14</b>	<b>0.18</b>
Quantum Efficiency (%)	72.1 (0.1)	88.3 (0.2)	92.4 (0.1)	86.4 (0.06)	73.0 (0.08)	59.1 (0.06)	14.2 (0.01)	3.9 (0.02)	1.7 (0.07)

Table S2. Refinement parameter of  $\text{Ga}_{1.994}\text{O}_3:0.006\text{Cr}^{3+}$ .

Crystal system	Monoclinic
Space group	<i>C2/m</i>
<i>Rwp</i>	1.65%
<i>Rp</i>	1.19%
$\chi^2$	2.31

Table S3. Lattice parameter of  $\text{Ga}_{1.994}\text{O}_3:0.006\text{Cr}^{3+}$ .

Atoms	x	y	z	$\frac{\text{O}_c}{\text{c}}$	Beq ( $\text{\AA}^2$ )
Ga1	0.08988(12)	0	0.79457(33)	1	0.033(53)
Ga2	0.34118(11)	0	0.68562(32)	1	0.022(52)
O1	0.16045(49)	0	0.1028(13)	1	0.11(19)
O2	0.49497(48)	0	0.2584(10)	1	0.03(17)
O3	0.82585(47)	0	0.4259(13)	1	0.03(15)
<i>a</i>			12.23328(24) $\text{\AA}$		
<i>b</i>			3.040145(57) $\text{\AA}$		
<i>c</i>			5.80791(12) $\text{\AA}$		
$\beta$			103.8331(15) $^\circ$		

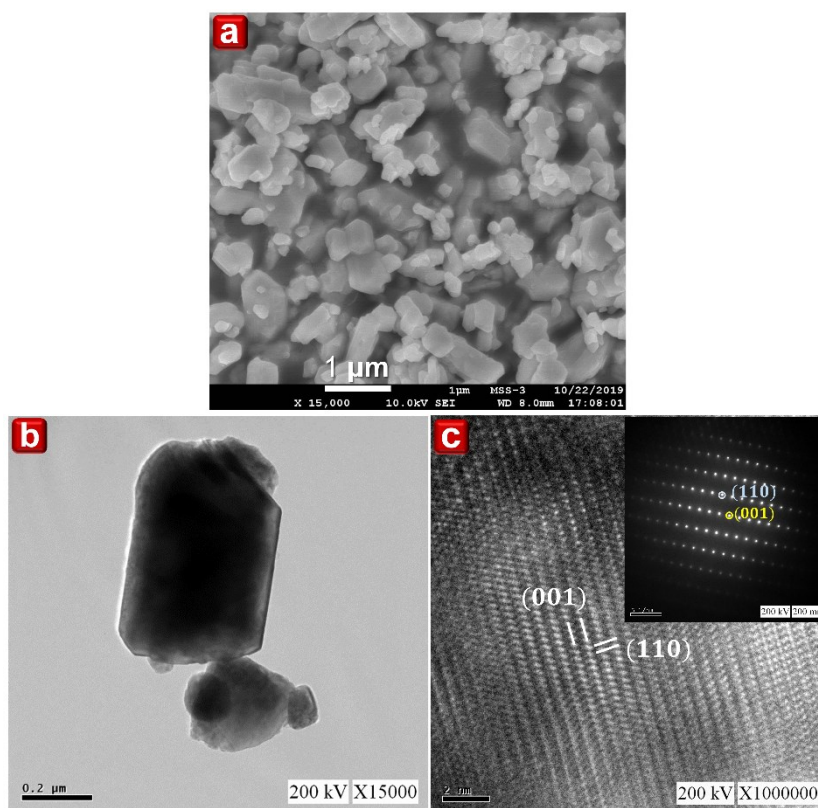


Figure S2. (a) SEM image of  $\text{Ga}_{1.994}\text{O}_3:0.006\text{Cr}^{3+}$ . (b) TEM of the  $\text{Ga}_{1.994}\text{O}_3:0.006\text{Cr}^{3+}$ . (c) HRTEM image of  $\text{Ga}_{1.994}\text{O}_3:0.006\text{Cr}^{3+}$  (the inset figure is the SAED pattern).

Table S4. Calculated and theoretical d-spacing of [001] and [110] from HRTEM.

	[001]	[110]	Interplane angle
<b>Experimental</b>	5.67 Å	3.04 Å	87.0
<b>Theoretical</b>	5.64 Å	2.95 Å	86.6

Table S5. Values of energy levels at ambient pressure and parameters of the crystal field model for Ga<sub>2</sub>O<sub>3</sub>:Cr<sup>3+</sup>.

Parameters	<sup>4</sup> A <sub>2</sub> → <sup>4</sup> T <sub>2</sub>	<sup>4</sup> A <sub>2</sub> → <sup>4</sup> T <sub>1</sub>	<sup>2</sup> E→ <sup>4</sup> A <sub>2</sub> (R1) E( <sup>2</sup> E)	ΔE (cm <sup>-1</sup> )	Dq (cm <sup>-1</sup> )	B (cm <sup>-1</sup> )	C (cm <sup>-1</sup> )	Δ' (cm <sup>-1</sup> )	Sħω (cm <sup>-1</sup> )
Values	16530 cm <sup>-1</sup> (605 nm)	22826 cm <sup>-1</sup> (438.1 nm)	14345 cm <sup>-1</sup> (697.1 nm)	6296	1653	620	3235	2185	1416

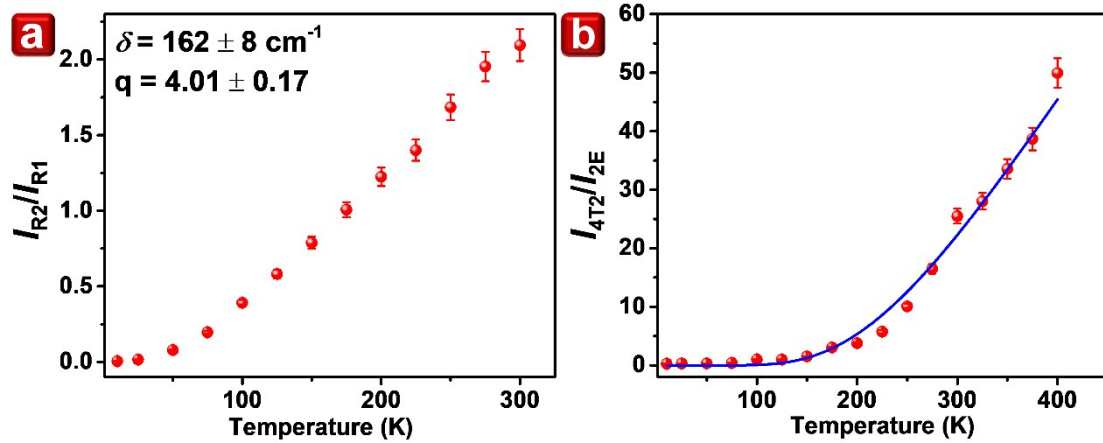


Figure S3. Temperature-dependent intensity ratio of R<sub>2</sub> and R<sub>1</sub> line emission and (b) the TDPL intensity ratio of the <sup>4</sup>T<sub>2</sub> → <sup>4</sup>A<sub>2</sub> and <sup>2</sup>E → <sup>4</sup>A<sub>2</sub> transitions of Ga<sub>1.994</sub>O<sub>3</sub>:0.006Cr<sup>3+</sup>.

### Pressure dependence of luminescence

Room-temperature pressure-dependent PL spectra of Ga<sub>2</sub>O<sub>3</sub>:Cr<sup>3+</sup> up to 190 kbar upon excitation at 442 nm are shown in Figure S4a. The shift of the maximum of broadband (<sup>4</sup>T<sub>2</sub>→<sup>4</sup>A<sub>2</sub>) emission spectra towards lower wavelength is observed for low pressure, while broadband emission disappears and only line emission is observed above 44 kbar. This is interpreted as the result of the pressure-induced shift of the <sup>4</sup>T<sub>2</sub> level towards higher energies. In effect, the thermal energy is too low at room temperature to induce the emission from <sup>4</sup>T<sub>2</sub> level, and <sup>2</sup>E state becomes the only emitting state. The change of relative intensity between R<sub>1</sub> and R<sub>2</sub> lines (Figure S4a) is observed. The R<sub>2</sub> line is no longer observed for pressure higher than 140 kbars.

Furthermore, the significant change of emission spectra between 123 and 140 kbars is observed and only one line is observed at the pressure above. Such phenomena are probably caused by the phase transition from  $\beta$ -Ga<sub>2</sub>O<sub>3</sub> to  $\alpha$ -Ga<sub>2</sub>O<sub>3</sub>, which was previously calculated at around 95 kbar.<sup>1</sup> Moreover, the experiment shows that for nanostructured material, this transition begins at 60 kbar and the nanocrystalline phase is a combination of both phases of gallium oxide for pressure between 60 and 150 kbar.<sup>2</sup> Energies of the R<sub>1</sub> and R<sub>2</sub> lines versus pressure are presented in Figure S4b. When pressure increases, the R-lines emission is shifted towards a higher wavelength. The values of pressure shifts were estimated for R-line emission, which is  $-0.81 \pm 0.04$  cm<sup>-1</sup>/kbar for R<sub>2</sub> emission up to 124 kbar,  $-1.8 \pm 0.1$  cm<sup>-1</sup>/kbar for R<sub>1</sub> emission up to 90 kbar, and  $-0.82$  cm<sup>-1</sup>/kbar from 90 to 190 kbar. The pressure-dependent decay profiles taken from the whole emission range up to 190 kbars, as shown in Figure S4c. The decay remain to be single exponential for lower pressure up to 88 kbar, while it becomes nonexponential for higher pressure. The decay curves for lower pressures were fitted using for the following equation:

$$I(t) = I_0 e^{-\frac{t}{\tau}} \quad (s1)$$

where  $I(t)$  is emission intensity at time  $t$ ,  $I_0$  is the initial intensity, and  $\tau$  is the decay time of the luminescence. The obtained decay time increases almost linearly and is 0.26 ms for 5 kbar and 2.90 ms for 88 kbar. According to the model presented the previous study, luminescence lifetime of octahedrally coordinated intermediate field Cr<sup>3+</sup> system, where the <sup>2</sup>E state is located slightly below the <sup>4</sup>T<sub>2</sub>, can be approximated by following formula:<sup>3</sup>

$$\tau = \frac{\left\{ 1 + \exp\left(-\frac{\delta}{kT}\right) + 3\exp\left(\frac{-\Delta}{kT}\right) \right\}}{\left[ \frac{1 + q \cdot \exp\left(-\frac{\delta}{kT}\right)}{\tau_E} + \frac{1}{\tau_T} 3\exp\left(\frac{-\Delta}{kT}\right) \right]} \quad (s2)$$

When pressure increases, the crystal field strength increases. As a result, the energy of <sup>4</sup>T<sub>2</sub> state increases, whereas the energy of <sup>2</sup>E slightly diminishes with pressure.<sup>4,5</sup>

Besides, the energies  $\Delta$  and  $\Delta'$  increase with pressure by quantities  $\frac{d\Delta}{dp}$  and  $\frac{d\Delta'}{dp}$ , respective. Pressure can change the quantity of  $S\hbar\omega$  depending on the lattice and dopant.  $S\hbar\omega$  can increase or decrease with increasing pressure.<sup>6</sup> Since we have no

information on the pressure-induced changes of electron lattice coupling  $S\hbar\omega$ , we can

assume that it is constant. Then, we assume that  $\frac{d\Delta}{dp} = \frac{d\Delta'}{dp}$ . We can modify equation (s2) to reproduce the pressure dependence of PL lifetime.

$$\tau = \tau_T \left[ \frac{1 + \exp\left(-\frac{\delta}{kT}\right) + 3\exp\left(-\frac{\Delta + \frac{d\Delta}{dp}}{kT}\right)}{\left\{\frac{V_{s-o}}{\Delta' + \frac{d\Delta}{dp}}\right\}^2 [1 + q \cdot \exp\left(-\frac{\delta}{kT}\right)] + 3\exp\left(-\frac{\Delta + \frac{d\Delta}{dp}}{kT}\right)} \right] \quad (s3)$$

To obtain relation (s3), we have assumed that spin-orbit interaction weakly depends on pressure. We performed the fitting to obtain the solid and dashed red curve, as

shown in Figure S4d. The fitted values for the red dashed curve were  $\frac{d\Delta}{dp} = 13.0 \text{ V cm}^{-1}/\text{kbar}$

obtained for  $\tau_T = 0.027 \text{ ms}$ ,  $\Delta = 630 \text{ cm}^{-1}$ ,  $\frac{\tau_E}{\tau_T} = \left\{\frac{\Delta'}{V_{s-o}}\right\}^2 = 125$ ,  $\delta = 162 \text{ cm}^{-1}$ , and  $q = 4$ . On the other hand, the best fit for the red solid curve, it has been obtained for  $\delta$

$= 162 \text{ cm}^{-1}$ ,  $q = 4$ ,  $\frac{\tau_E}{\tau_T} = \left\{\frac{\Delta'}{V_{s-o}}\right\}^2 = 125$ , and  $\tau_T = 0.027 \text{ ms}$ , where fitting parameters were

$\frac{d\Delta}{dp} = 10 \pm 0.5 \text{ cm}^{-1}/\text{kbar}$  and  $\Delta = 880 \pm 30 \text{ cm}^{-1}$ .

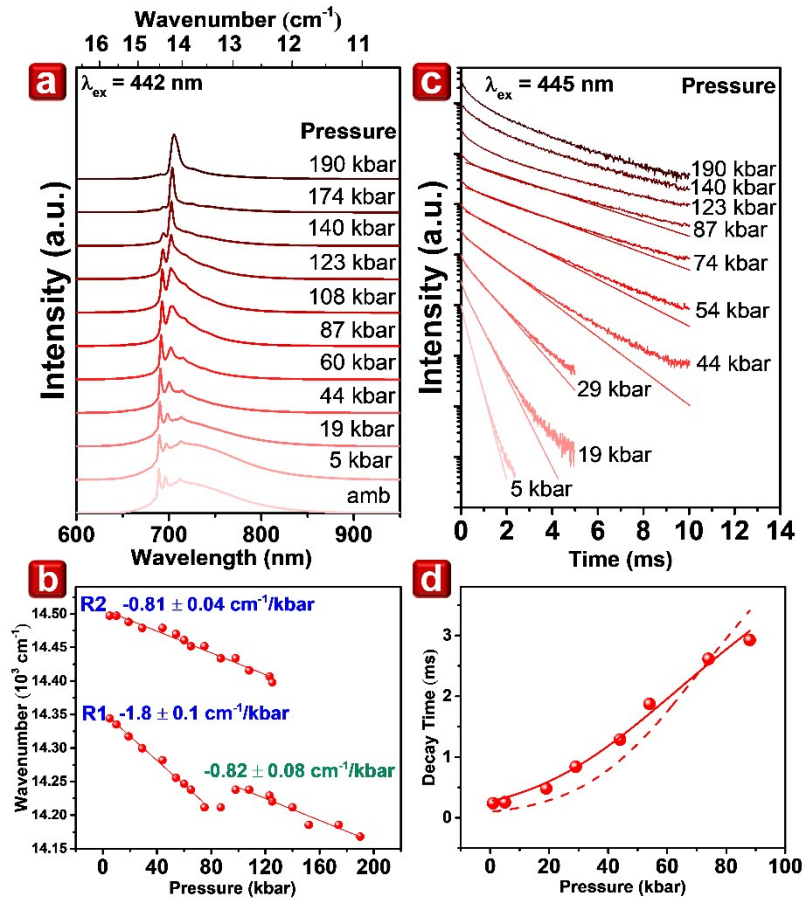


Figure S4. Pressure-dependent (a) emission spectra upon excitation at 442 nm, (b) pressure shift of the R<sub>1</sub> line and R<sub>2</sub> line vs. pressure in wavenumber scale, (c) pressure-dependent decay profiles upon excitation at 445 nm and (d) calculated decay times of

Ga<sub>2</sub>O<sub>3</sub>:Cr<sup>3+</sup>. The dashed curve is convoluted by using relation S3 and  $\Delta = 630$  and  $\frac{d\Delta}{dp} = 13.0 \text{ cm}^{-1}/\text{kbar}$ , and solid curve by using  $880 \text{ cm}^{-1}$  and  $\frac{d\Delta}{dp} = 10.0 \text{ cm}^{-1}/\text{kbar}$ .

### Electron Paramagnetic Resonance

The EPR technique allows determining the nearest surroundings of paramagnetic ions. The EPR spectrum from chromium ions is observed in the positions  $g \sim 4$  and  $g \sim 2$ , depending on the crystal field surrounding these ions. The signal is observed in strong magnetic inductions region ( $g \sim 2$ ) in weaker crystal fields, while it is observed in weaker magnetic inductions ( $g \sim 4$ ) in strong crystal fields. Cr<sup>3+</sup> ions have an electron spin  $S = 3/2$ , so powder compounds can be characterized by many EPR lines depending on the symmetry of these ions and the nearest environment (interactions between chromium ions). Here, we observe the signal in the entire range of magnetic induction

from 10 mT to 550 mT. Several transitions in strong ( $g = 5.54, 5.01$ ), medium ( $g = 2.46$ ) and weak ( $g = 1.57$ ) magnetic induction are clearly observed, as shown in Figure S5.

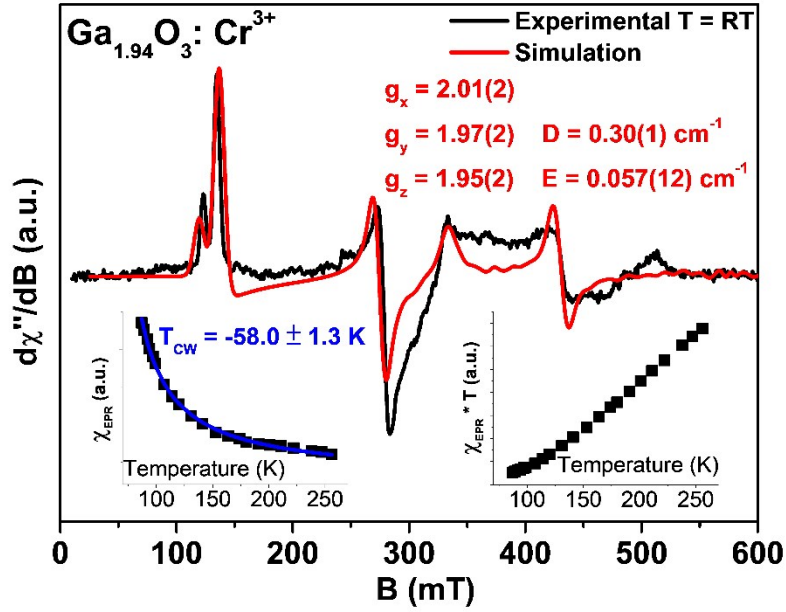


Figure S5. Experimental and simulated EPR spectrum of  $\text{Ga}_2\text{O}_3:\text{Cr}^{3+}$  at room temperature. The inset shows the dependence of magnetic susceptibility, Curie-Weiss parameters (left side), and magnetic moment (right side) on temperature.

Based on the experimental data, the parameters of spin Hamiltonian (SH) were determined from the following equation, consisting the Zeeman (Z) and Zero Field Splitting (ZFS) terms:

$$H = H_Z + H_{ZFS} = \mu_B B \cdot g \cdot S + D \left( S_z^2 - \frac{1}{3} S(S+1) \right) + E (S_x^2 + S_y^2)$$

where  $\mu_B$  – Bohr magneton,  $B$  – induction of magnetic field,  $g$  – effective spectroscopic splitting factor,  $S$  – electron spin,  $D$  – axial and  $E$  – rhombic distortions of octahedral. We have obtained the following values of the Zeeman parameters  $g_x = 1.95(2)$ ,  $g_y = 1.97(2)$ ,  $g_z = 2.01(2)$  ( $g_x \approx g_y \neq g_z$ ), indicating an axial symmetry of the chromium ion environment. The zero-field splitting (ZFS) parameters,  $D = 0.30(1) \text{ cm}^{-1}$ ,  $E = 0.057(12) \text{ cm}^{-1}$  indicate significant axial distortion of the  $C_4$  symmetry. The results of the fitting of SH parameters by using the least square's method are shown in Figure S5.

Temperature dependence of the integrated EPR intensity is presented in the inset of Figure S5. The EPR integrated intensity,  $\chi_{\text{EPR}}$ , is defined as an area under the absorption EPR spectrum and is proportional to the magnetic susceptibility of the

investigated spin system. For many paramagnetic ions, the temperature dependence of the integrated intensity is accurately described by the Curie-Weiss law,  $\chi_{\text{EPR}}(T) = C/(T-T_{\text{CW}})$ , where  $T_{\text{CW}}$  is the Curie-Weiss constant. The Curie-Weiss law appears to be valid at the entire temperature range. The least-square fitting of the experimental points to the Curie-Weiss law produced  $T_{\text{CW}} = -58$  K. The negative sign and a large value of the Curie-Weiss temperature indicate a strong antiferromagnetic interaction between chromium ions. The temperature dependence of the product of temperature and integrated intensity,  $T \cdot \chi_{\text{EPR}}$ , is depicted in the inset of Figure S5. In general, this product is proportional to the square of an effective magnetic moment. For  $\text{Ga}_2\text{O}_3:\text{Cr}^{3+}$ , the magnetic moment decreases with temperature in the entire temperature range, which is in line with our expectation. This confirms the strong antiferromagnetic interactions between the chromium ions.

### **Chemical Stability**

The luminescent degradation is also an important issue to evaluate its potential for the practical application. To understand the chemical stability of  $\text{Ga}_2\text{O}_3:\text{Cr}^{3+}$ , the relative quantum efficiency is measured by putting the powder in the oven with the temperature and humidity of 85 °C and 85%, respectively, as shown in Figure S6.  $\text{Ga}_2\text{O}_3:\text{Cr}^{3+}$  can maintain 95% of its original quantum efficiency after 7 days, revealing its good stability toward the moisture and the great potential for the practical application.

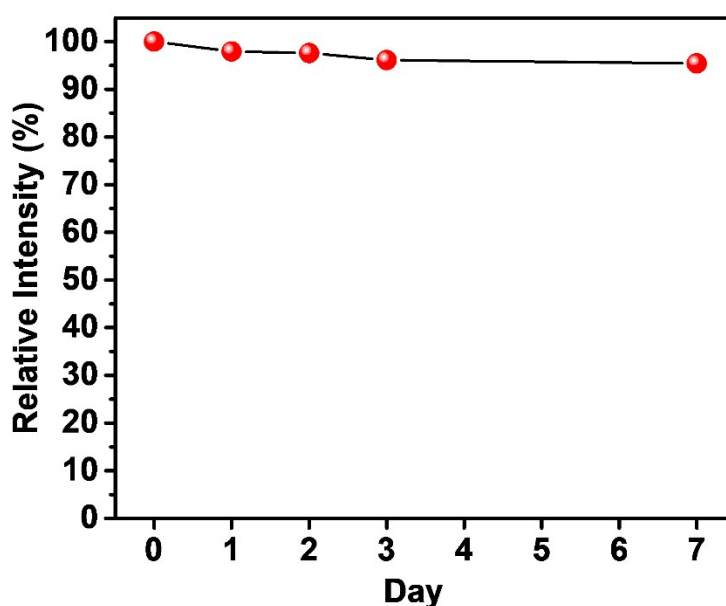


Figure S6. Relative quantum efficiency of Ga<sub>2</sub>O<sub>3</sub>:Cr<sup>3+</sup> under the condition of 85 °C and 85% humidity.

### References

1. H. He, R. Orlando, M. A. Blanco, R. Pandey, E. Amzallag, I. Baraille and M. Rérat, *Phys. Rev. B*, 2006, **74**, 195123.
2. K. Lipinska-Kalita, B. Chen, M. Kruger, Y. Ohki, J. Murowchick and E. Gogol, *Phys. Rev. B*, 2003, **68**, 035209.
3. M. Grinberg, T. Lesniewski, S. Mahlik and R. S. Liu, *Opt. Mater.*, 2017, **74**, 93-100.
4. M. Grinberg and A. Suchocki, *J. Lumin.*, 2007, **125**, 97-103.
5. Z. Zhang, K. T. Grattan and A. W. Palmer, *Phys. Rev. B*, 1993, **48**, 7772.
6. M. Grinberg, J. Barzowska, Y. Shen, R. S. Meltzer and K. L. Bray, *Phys. Rev. B*, 2004, **69**, 205101.